Self-referenced prism deflection measurement schemes with microradian precision

Rebecca Olson, Justin Paul, Scott Bergeson, and Dallin S. Durfee

We have demonstrated several inexpensive methods that can be used to measure the deflection angles of prisms with microradian precision. The methods are self-referenced, where various reversals are used to achieve absolute measurements without the need of a reference prism or any expensive precision components other than the prisms under test. These techniques are based on laser interferometry and have been used in our laboratory to characterize parallel-plate beam splitters, penta prisms, right-angle prisms, and corner cube reflectors using only components typically available in an optics laboratory. © 2005 Optical Society of America

OCIS codes: 120.2650, 120.3180, 120.3940, 230.1360, 230.5480.

1. Introduction

Reflecting prisms are key components in a variety of optical instruments. They can be used in place of mirrors to alter the direction of optical beams. Unlike mirrors, however, prisms can be used in such a way that the angle through which the beam is deflected does not change when the optic is rotated. For example, after a beam reflects off of the three perpendicular surfaces of a corner cube it will exit the prism traveling in precisely the opposite direction as the incoming beam. No careful alignment is needed to achieve this nearly perfect 180 deg deflection. Reflecting prisms are useful in situations where it is difficult to perform the initial alignment or when it is critical to maintain a particular beam deflection for a long period of time. One well-known example is use of corner reflectors for lunar ranging experiments.[1] Our interest in prisms is to generate an extremely stable array of laser beams for use in an atom interferometer.

Since the beam deflection is determined by the angles between the prism surfaces rather than the alignment of the optic, it is extremely important that the prisms be made correctly. Several methods are commonly used to measure deflection angles of prisms.[2–4] One class of techniques utilizes telescopes and autocollimators to image the separation of two beams at infinity. Our methods are based on a second class in which the angle between the two beams is ascertained using optical interference. Both types of measurement are limited by the size of the beam of light passing through the optics, in the first case by Rayleigh's criterion and in the second by the large fringe spacing resulting from nearly parallel beams. As such, both types of measurement have similar ultimate resolution limits. Techniques based on either type of measurement typically require a calibrated reference prism or other expensive optical components.

After purchasing a set of extremely high-precision prisms for use in an atom interferometer, we began to have doubts as to whether the manufacturer had met our required specifications. Not having access to an instrument capable of measuring prism deflection angles to the necessary accuracy, we developed a set of techniques that allow prism deflection angles to be measured with accuracies of a few microradians. Our scheme is self-referencing, requiring no calibrated prism. In addition to the prisms under test we needed only several standard-quality mirrors, lenses, and attenuators, an inexpensive alignment laser, a low-quality surveillance camera, and for some measurements a piezoelectric transducer (PZT). We characterized parallel-plate beam splitters (which generate two precisely parallel beams), penta prisms (which deflect light by 90 deg), right-angle

When this research was performed, the authors were with the Department of Physics and Astronomy, Brigham Young University, Provo, Utah 84602. R. Olson is now with the Department of Physics, University of Maryland, College Park, Maryland 20742. D. S. Durfee's e-mail address is dallin_durfee@byu.edu.

Received 1 November 2004; revised manuscript received 11 March 2005; accepted 31 March 2005.

0003-6935/05/224639-09$15.00/0

© 2005 Optical Society of America

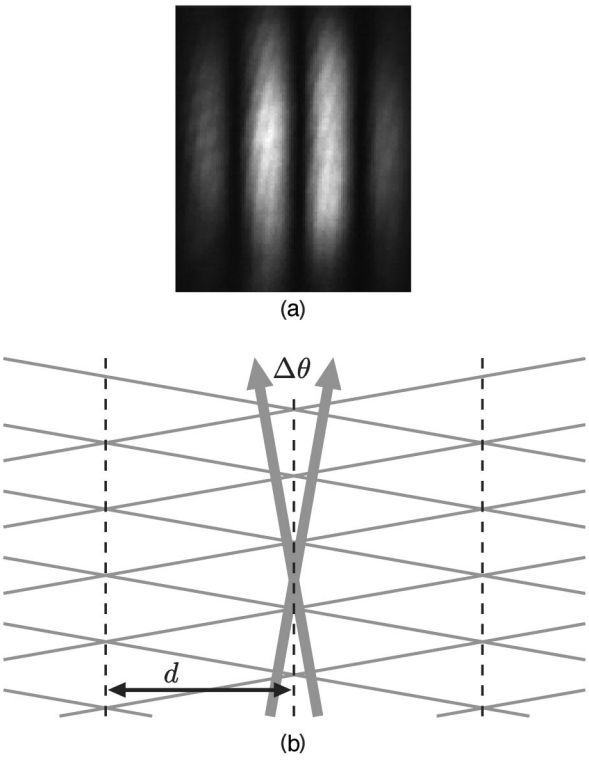

Fig. 1. Fringes formed by two crossing plane waves. In (a) the interference pattern formed when two beams from a He–Ne laser crossed at a small angle is shown. In (b) the gray arrows represent the propagation or k vectors of the two plane waves, and the thin gray lines represent the wave fronts of the two traveling waves. The angle between the propagation vectors of the two beams is labeled as $\Delta\theta$. The interference maxima, where the two waves are always in phase, are denoted with the dashed lines, and the spacing between the interference maxima is labeled as d.

prisms (which fold light by 180 deg in the plane of the prism), and corner cubes.

Our methods utilize optical interferometry and bear similarity to the Jamin interferometer.[5] Like several other schemes, in our methods the deflection angles of prisms are determined from the spacing between fringes formed by two interfering beams. Each of our designs produces similar intensities for the two interfering beams, resulting in high-contrast fringes for maximum sensitivity. Lenses and mirrors are used only before the beams are split or after the interference pattern is formed such that alignment or wave-front errors due to these optics have a negligible effect on the measurements.

2. Measuring the Angle between Two Beams

When two monochromatic plane waves intersect, they form an interference pattern. Because the spacing between interference fringes depends on the angle between the two wave vectors, it is possible to ascertain the angle between the two propagation directions by analyzing the fringe pattern. Using Fig. 1 and simple trigonometry, it is easy to find a relationship between the fringe spacing d and the angle between the k vectors of the two plane waves $\Delta\theta$. In the small-angle approximation, for two plane waves with wavelength λ projected onto a screen at near-normal incidence, the angle between the two beams is given by

$$\Delta\theta = \lambda/d. \tag{1}$$

A. Fitting to a Piece of a Fringe

Most of the optics we tested have a clear aperture of 2.5 cm. To prevent clipping we made our measurements using a helium–neon laser ($\lambda = 633$ nm) collimated to a diameter of $\sim$1 cm, suggesting that we would only be able to measure fringe spacings if the fringes were less than 1 cm apart. According to Eq. (1) this limit on d results in a minimum measurable $\Delta\theta$ of 0.13 mrad. The optics we measured were specified to have angular tolerances of a few microradians. To make measurements with microradian precision, we had to infer angles from images that contained much less than one fringe.

One method commonly used in this situation is phase shifting, in which intensity is measured at several points as the fringe pattern is scanned across the points by shifting the phase of one beam.[6] This method has several advantages over the spatial fringe-fitting method used in our experiments: It is less susceptible to wave-front distortion, it reveals the sign of the angle between the beams (not just the magnitude), and it can be used for other types of measurement (such as surface profiling) that cannot easily be done with the method we chose. But our spatial fringe-fitting method has the advantage that all the data are recorded in a single moment, making it more robust in noisy environments. It also does not require the incorporation of a phase-shifting device, reducing cost and complexity and eliminating potential errors due to phase-shifter beam deflections, drifts, and hysteresis. Adding a phase shifter would have greatly complicated our scheme for the measurement of plate beam splitters. In our other schemes it could have been implemented by scanning one prism with a PZT. As discussed in Subsection 3.B, we used a PZT in some of our schemes for other purposes, but they lacked sufficient stability for this purpose [see Fig. 7(a)].

To find the angle between the two beams, we simply curve fit the intensity pattern on our camera. But to get accurate results when less than one fringe is visible, we have to take into account the spatial profiles of the beams. To do this we first write down the expression for the electric field of a laser beam as a function of the position on the camera $\mathbf{r}$ and time t. To simplify our analysis we assume that the interfering beams have the same polarization. We also assume that the two beams are well collimated such that the phase of each beam's electric field is of the form $\mathbf{k}\cdot\mathbf{r} - \omega t + \phi$ where $\mathbf{k}$ is the wave vector of the beam, ω is the angular frequency of the light field, and ϕ is a constant phase offset. With these assumptions, the electric field of each beam can be written as

$$E_n(\mathbf{r},\ t) = f_n(\mathbf{r})\cos(\mathbf{k}_n\cdot\mathbf{r} - \omega t + \phi_n), \tag{2}$$

where $f_n(\mathbf{r})$ is the amplitude of the electric field at position $\mathbf{r}$ and the subscript n is equal to 1 or 2 depending on which of the interfering beams we are describing.

The intensity of the interference pattern of two intersecting beams is related to the time average of the square of the sum of the two interfering electric fields. When the time average is evaluated and the equation is simplified, it can be expressed as

$$I_{12}(\mathbf{r}) = I_1 + I_2 + 2(I_1 I_2)^{1/2} \cos(\mathbf{k}_{\text{rel}} \cdot \mathbf{r} + \Delta\phi), \qquad (3)$$

where $\Delta\phi = \phi_1 - \phi_2$ and $\mathbf{k}_{\text{rel}} = \mathbf{k}_1 - \mathbf{k}_2$, and where I_1 and I_2 are the intensity patterns that would be measured on the camera if only one of the two interfering beams was present.

Without losing generality we can define the plane of the camera's detector to be the $z = 0$ plane (such that $\mathbf{r}$ has no z component). Then we can write the dot product $\mathbf{k}_{\text{rel}} \cdot \mathbf{r}$ as $k_x x + k_y y$ where x and y are Cartesian coordinates describing the location of pixels on our camera and k_x and k_y are the spatial frequencies of the interference pattern imaged by the camera. If both beams strike the camera near to normal incidence, then the z component of $\mathbf{k}_{\text{rel}}$ will be nearly zero and k_{rel} will be approximately equal to $(k_x^2 + k_y^2)^{1/2}$. These definitions result in the following expression:

$$\frac{I_{12} - I_1 - I_2}{2(I_1 I_2)^{1/2}} = \cos(k_x x + k_y y + \Delta\phi). \qquad (4)$$

The left-hand side of Eq. (4) can be thought of as a normalized intensity.

If the two beams are nearly parallel, it can be shown that $k_{\text{rel}} \simeq 2\pi\Delta\theta/\lambda$. To find $\Delta\theta$ we simply measure I_{12}, I_1, and I_2 and numerically fit the left side of Eq. (4) to the right side to find k_x and k_y, treating $\Delta\phi$ as a free parameter. We then calculate k_{rel} and from that $\Delta\theta$. The three intensity patterns needed to calculate the left side of Eq. (4) are measured by taking four images: one of the two interfering beams, one of beam 1 with beam 2 blocked, one of beam 2 with beam 1 blocked, and a dark field image with both beams blocked. An example of a set of images is shown in Figs. 2(a)–2(d). We then subtract the dark field image from the other three to generate the three background-free intensity patterns I_{12}, I_1, and I_2. The separate I_1 and I_2 terms in Eq. (4) make this measurement technique work even if the fringes have low contrast due to mismatched power in the two interfering beams. Lower contrast does increase digitization noise, which is of special importance when a low-bit-depth camera is used. This technique also works if the interfering beams do not overlap perfectly, although misalignments can reduce the region of useful data [see Fig. 2(e)]. Large overlap misalignments coupled with wave-front curvature in the beams can also add errors to the measurements.

Figure 2(e) shows the result of this calculation applied to the data in Figs. 2(a)–2(d). Curve fits to find k_x and k_y from this data are illustrated in Figs. 3(a) and 3(b). Although the data in Fig. 3 are somewhat noisy, we can still get accurate, repeatable results by applying the constraint that the normalized interference pattern on the left-hand side of Eq. (4) should oscillate with unity amplitude and zero offset. This is clearly evidenced by the consistency of the measurements shown in Fig. 7 in Section 3.

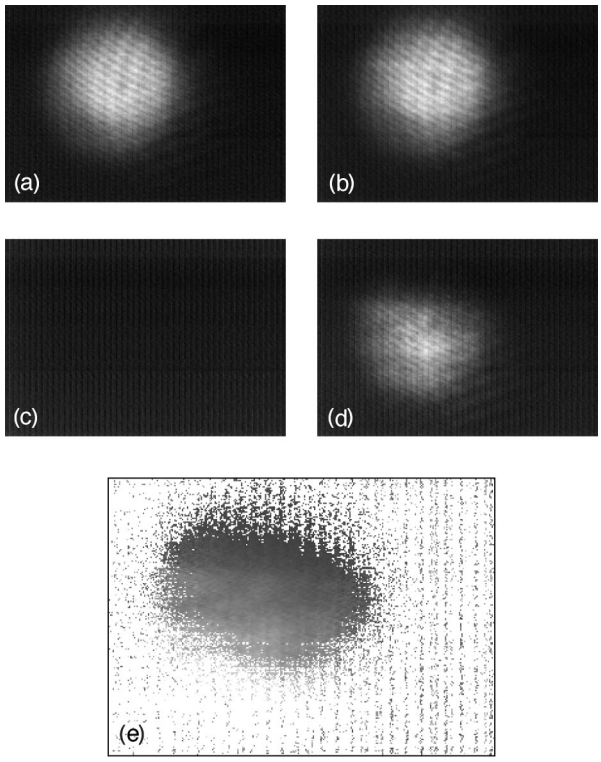

Fig. 2. Calculation of the normalized interference pattern. Images (a)–(d) are an example of the four images that are needed to evaluate Eq. (4). Frames (a) and (b) are images of the individual beams with the other beam blocked, (c) is a dark field with both beams blocked, and (d) is an image of the two beams interfering. The closely spaced interference lines visible in these images are low-contrast fringes due to reflections off of the camera window and the focusing lens. The high-contrast fringes due to the angle between the two beams are not apparent in the interference frame because the spacing between fringes is larger than the size of the beams. Plugging the data from these images into the left-hand side of Eq. (4) results in the image shown in (e). Only the central part of (e), where both beams are present, contains meaningful information. The shading scale in (e) runs from −1.35 (pure black) to 0.05 (pure white).

B. Experimental Subtleties

When using this curve-fitting approach to measure deflection angles of prisms, we often made small adjustments to the prism or beam-splitter alignment to shift the relative phase of the two interfering beams such that images were not centered on a light or dark fringe. Only small adjustments that did not affect the overlap of the interfering beams were needed. Capturing data between a light and a dark fringe results in a more precise fit to the data. Fitting data near an extremum of the cosine requires precise measure-

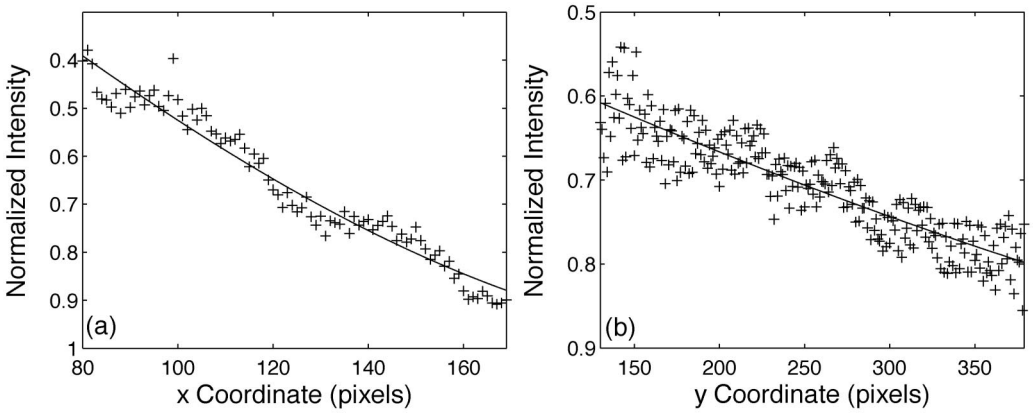

Fig. 3. Curve fits to find the angle between two beams. Strips through the center of the data from Fig. 2(e) are shown, along with least-squared fits to the functions $\cos(k_x x + \phi_x)$ and $\cos(k_y y + \phi_y)$. The deviation of the data from the fits is largely due to camera window reflections. These higher-spatial-frequency, low-contrast fringes average away to a large extent in the curve fit.

ment of the curvature of the data. Near a zero crossing, however, simply extracting the slope of the data is enough to get a good measurement of k.

In our treatment we have assumed a well-collimated laser beam and have ignored effects of wave-front curvature. To ensure good beam collimation, we constructed a simple Michelson–Morley interferometer with mismatched arms, one arm being ~2 cm long and the other over 1 m long. The interferometer was aligned to create a circular interference pattern. We then adjusted the lenses used to telescope up the size of the laser beam until no interference rings were visible. When measuring prism deflection angles, we made sure that the two optical paths were the same length on a millimeter scale and that the two interfering beams hit the camera at nearly the same place. This made any residual wave-front curvature common to both field components such that it did not affect our results.

The detector on the camera used in these experiments was smaller than the laser beam diameter. Since catching only part of the interference pattern limits sensitivity to small relative beam angles, we used a lens to demagnify the pattern. To account for the demagnification and to find the correct effective size of the camera pixels, we placed a ruler in front of the lens. The ruler's position was adjusted until it came into clear focus on the camera. We then took pictures of the ruler to determine the magnification due to the lens. We verified that this had been done correctly by using the lens' focal length and the distance to the camera to calculate the position at which we would expect the ruler to come into focus and the expected magnification.

When we evaluated the left-hand side of Eq. (4) we had to be careful to utilize only the parts of the images where sufficient laser light was present in both beams to avoid large errors due to division by small numbers [see Fig. 2(e)]. We designed our software to prompt the user to select a region of interest to avoid regions of low intensity. The left-hand side of Eq. (4) is then computed in this region. The software then fits a horizontal row of data in the middle of the selected region to the function $\cos(k_x x + \phi_x)$ and fits a vertical column of data in the middle of the region to the function $\cos(k_y y + \phi_y)$. From these two one-dimensional fits, it calculates k_{rel} and determines the angle between the beams.

3. Measuring Prism Beam Deflections

In this section we discuss several methods that we used to characterize the properties of parallel-plate beam splitters, penta prisms, right-angle prisms, and corner cubes. We tested uncoated optics. Light intensity was lost because of imperfect transmission each time a beam entered or exited a prism. Much larger losses occurred because of missing reflective coatings on the beam splitters and the penta prisms (right-angle prisms and corner cubes do not require reflective coatings due to total internal reflection). But even with these losses we could still saturate the camera. Balancing the intensities of the two interfering beams was necessary to achieve high-contrast fringes to get the most accuracy with the fixed bit-depth of our camera. Our methods have symmetric losses in each beam, resulting in well-matched beam intensities.

A. Absolute Beam-Splitter Characterization

The beam splitters we measured were uncoated plates of BK7 glass with parallel surfaces. As shown in Fig. 4, when a laser beam passes through an uncoated piece of glass, surface reflections result in multiple beams exiting the glass. We are concerned only with the beam that passes through without reflecting and the nearly parallel beam resulting from one reflection from each surface (labeled 1 and 2 in Fig. 4). If the two beam-splitter surfaces are exactly parallel, these two beams will emerge exactly parallel. Otherwise there will be an angle θ between the two exiting beams (see Fig. 4). By measuring θ, the prism wedge angle ψ can be inferred.

The relationship between θ and ψ can be found using Snell's law and the law of reflection. If beam 1

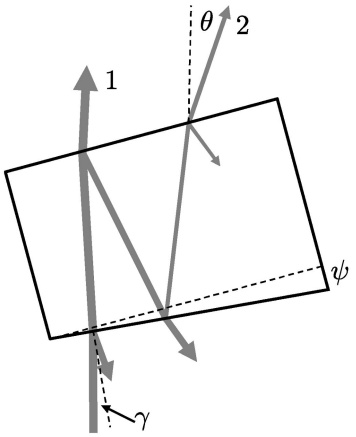

Fig. 4. Generation of two nearly parallel beams with a plate beam splitter. The gray lines represent laser light. Light enters the beam splitter in the lower left-hand corner. At each interface the beam is split into a reflected and a transmitted beam. For most of our studies we are interested only in the two beams exiting the beam splitter that are labeled 1 and 2. The angle between the incoming beam and the normal of the first surface is labeled as γ, the angle between beams 1 and 2 is labeled as θ, and the wedge angle of the glass plate is labeled ψ.

in Fig. 4 defines the z axis and the x axis is defined such that the angle γ is in the x–z plane, in the limit of small wedge angles the x component of ψ is related to the x component of θ by

$$\psi_x = \frac{\theta_x}{2}\left[\frac{1-\sin^2(\gamma)}{n^2-\sin^2(\gamma)}\right]^{1/2}, \tag{5}$$

where n is the index of refraction of the beam splitter. The y component of ψ is given by the same relationship, with ψ_y and θ_y replacing ψ_x and θ_x.

To measure the wedge angle of parallel-plate beam splitters we used the configuration shown in Fig. 5. In this configuration two beam splitters form a Mach–Zehnder interferometer. Since each of the two beams undergoes two reflections, the two interfering beams have similar intensities, resulting in high-contrast interference fringes. To obtain a good overlap between the interfering beams and to make the Fresnel coefficients the same in both beam splitters, the two beam splitters were placed at similar angles relative to the incoming beam.

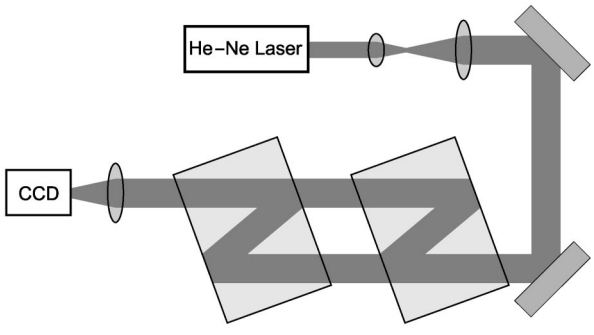

Fig. 5. Optical setup to measure the wedge angles of parallel-plate beam splitters.

In this arrangement the interference pattern does not reveal the wedge angle of a single beam splitter, but gives a combination of the wedge angles of both beam splitters. To find the wedge angle of a single beam splitter, we make four measurements using different combinations of three beam splitters and use the fact that flipping a beam splitter over effectively reverses the sign of its wedge angle. The first and second measurements use beam splitters A and B, with beam splitter B turned over between measurements. The third and fourth measurements use beam splitters A and C, with beam splitter C turned over between them. In each of the four configurations we measure the k_x and k_y of the interference pattern to extract the magnitude of the x and y components of the angle between the outgoing interfering beams using the methods discussed above.

If θ_{Ax}, θ_{Bx}, and θ_{Cx} represent the x components of the relative deflection errors of beam splitters A, B, and C, and the magnitudes of the x components of the angle between the interfering beams in the four measurements are represented by M_{1x}, M_{2x}, M_{3x}, and M_{4x}, the four measurements yield the following results:

$$M_{1x} = \theta_{Ax} - \theta_{Bx}, \tag{6}$$

$$\pm M_{2x} = \theta_{Ax} + \theta_{Bx}, \tag{7}$$

$$\pm M_{3x} = \theta_{Ax} - \theta_{Cx}, \tag{8}$$

$$\pm M_{4x} = \theta_{Ax} + \theta_{Cx}. \tag{9}$$

A similar set of equations can be written for the y components. Fitting our data with Eq. (4) does not reveal the sign of the angle between the two interfering beams. But we can assume a convention in which the angle between the two interfering beams is defined to be positive for our first measurement. For the following measurements we must stick to the same convention. The ± sign in the lower three relations therefore results from the uncertainty in the sign of the angle between the interfering beams when they are measured interferometrically.

The equations can be solved for the x component of the relative deflection angle of each beam splitter as a function of the four measured angles. But without knowledge of the sign of the angle between the interfering beams, these expressions cannot be evaluated. Fortunately, the above system of four equations yields two independent expressions for θ_{Ax}, one in terms of M_{1x} and M_{2x} and the other in terms of M_{3x} and M_{4x}. In most cases the requirement that θ_{Ax} be the same as determined by both equations unambiguously determines the sign of each measurement term. Once the signs are determined, the wedge angle for each of the three beam splitters can be determined. Using this technique we characterized several high-precision beam splitters, measuring wedge angles from 1 to 6 μrad.

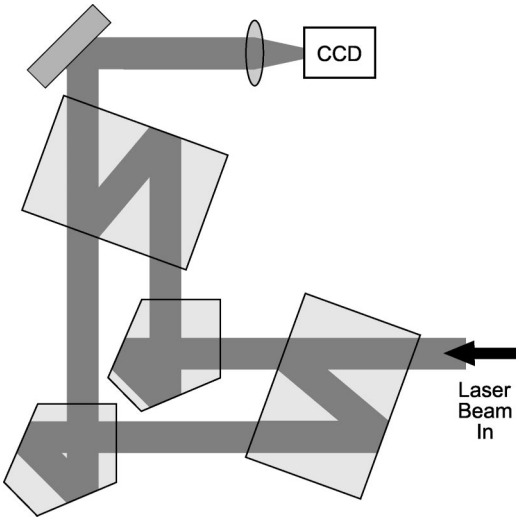

Fig. 6. Optical setup to measure relative deflection angles of penta prisms.

B. Relative Penta Prism Characterization

Our application does not place tight requirements on the absolute angular deflection produced by our penta prisms. It does, however, require that pairs of penta prisms be precisely matched. As such we measured the relative deflection of each matched pair rather than the absolute deflection of individual prisms. We did this using the optical configuration shown in Fig. 6. In this configuration one of the plate beam splitters, characterized using the methods described above, was used to generate two parallel beams. These beams were then folded at right angles using a pair of penta prisms. The two beams were then recombined using a second plate beam splitter.

In this layout the two beam paths are symmetric, allowing us to make the two path lengths nearly the same and making for equal intensity losses in each beam as they reflect off of our uncoated prisms. We used the same angle of incidence for both beam splitters to make the Fresnel coefficients equal. To get the two interfering beams to overlap, we adjusted the separation of the penta prisms to make the spacing between the two beams entering the second beam splitter equal to the spacing of the two beams exiting the first beam splitter.

Penta prisms ensure deflection of a beam by a precise angle in the plane of the prism. If, however, one prism is tilted out of the plane defined by the other prism, the two interfering beams would be at an angle to one another determined not by the accuracy of the prisms but by their relative alignment. For small misalignments we can think of the light deflection by the second prism as a fixed deflection in the plane defined by the first prism plus an out-of-plane deflection due to misalignment. As such, the magnitude of the wave vector describing the sinusoidal interference pattern measured at the output would equal the quadrature sum of two orthogonal components: a component due to errors in the manufacture of the prisms and a component due to the relative alignment of the prisms, as shown in Eq. (10):

$$k_{\mathrm{rel}} = (k_p{}^2 + k_a{}^2)^{1/2}. \tag{10}$$

Here k_p represents the component due to the error in the prism, and k_a represents the component due to the alignment error.

Because k_{rel} is at a minimum when there is no alignment error (i.e., when $k_a = 0$), it is possible to measure k_p by making measurements while adjusting the out-of-plane alignment of one prism. Rather than searching for a minimum value, we took several measurements at different alignments and fit our measurements to the form of equation Eq. (10) to extract an accurate value for k_p. To do this we mounted one of our prisms on a PZT mount that enabled fine alignment adjustments. We would manually adjust the alignment such that the minimum of k_{rel} occurred near the middle of the range of our PZT. We then took images as we scanned the PZT.

Because our fringe analysis method utilizes data taken at a single moment in time, we were able to make precise measurements of k_p even though our PZT was unstable. Assuming that k_a will be proportional to the voltage V applied to the piezoelectric element, we can take the measured k_{rel} as a function of V and perform a curve fit to find k_p. This curve fit requires two free parameters (in addition to k_p): the voltage at which $k_a = 0$ and the constant of proportionality between V and k_a. As shown in Fig. 7(a), however, because of the nonlinearity and drift in our piezoelectric mount, the data do not fit the hyperbolic form of Eq. (10) well. But since the k_p component was approximately in the horizontal plane of our camera and k_a was in the vertical, we could perform much better fits when we plotted the total k_{rel} versus k_y, the vertical component of k_{rel} extracted by our image analysis software. These fits had no free parameters. Typical curve fits are shown in Figs. 7(b) and 7(c).

The fit in Fig. 7(b) yields a k_p of 64.4 rad/m corresponding to a relative deflection angle of 6.5 μrad for the two prisms with a rms fit error corresponding to 0.38 μrad. Scanning the PZT had the side effect of moving the location of bright and dark fringes such that some images contained an extremum. But comparing the data points in Fig. 7(b) that contain an extremum to those that did not, it is clear that this did not significantly reduce the accuracy of the fits. A fit in which we use just the data for which the image did not contain an interference minimum or maximum gives a relative deflection of 7.5 μrad. Although most of the information in the plots is contained in the lowest points where the hyperbola is dominated by k_p, simply fitting to the two points at the extremes of the scan gives a reasonable relative deflection of 6.8 μrad, implying that only a small number of images are needed to get accurate results. Similar results were seen for our other prism pairs, suggesting a repeatability of this method at the microradian level. Because of the known deflection error of the beam splitters used in these measurements, the ab-

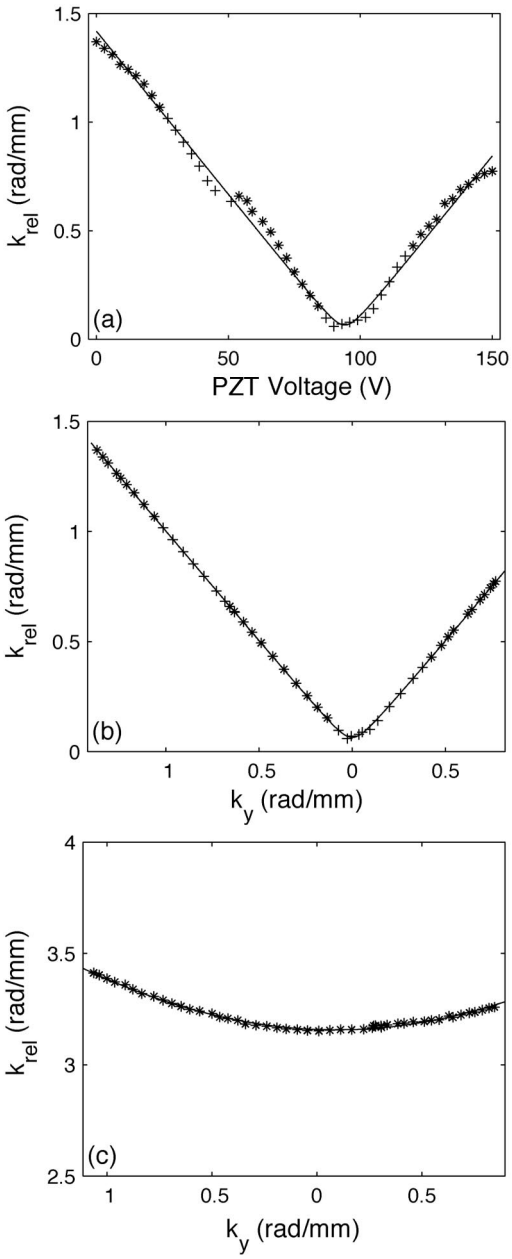

Fig. 7. Finding the relative deflection error of two penta prisms. The magnitude of the wave vector describing the interference pattern at different prism alignments is plotted versus (a) the PZT voltage and (b) the y component of the wave vector. The crosses and the asterisks represent the actual data extracted from the interference patterns. The asterisks represent the data points that should be the most accurate since the image happened to fall between a light and a dark fringe. The crosses represent data points for which the image contained a light or dark extremum. The curves represent equally weighted least-squares fits of the entire data set to Eq. (10). Data from a different set of prisms that did not meet our specifications are shown in (c).

solute accuracy of our measurements was limited to ~ 2 μrad.

The consistency of the data in Fig. 7 gives a good idea of the overall accuracy of our fringe measurement technique. One sign of self-consistency is the fact that the asymptotes of the hyperbola in Fig. 7(b) cross at a value of k_{rel} that is very close to zero. In all our measurements of precision prism pairs we measured offsets corresponding to angle measurement errors ranging from nearly zero to 1.02 μrad. Another indication of the accuracy of our fringe analysis is the low rms error of the curve fits to Eq. (10). These ran from 0.40 to 1.24 μrad.

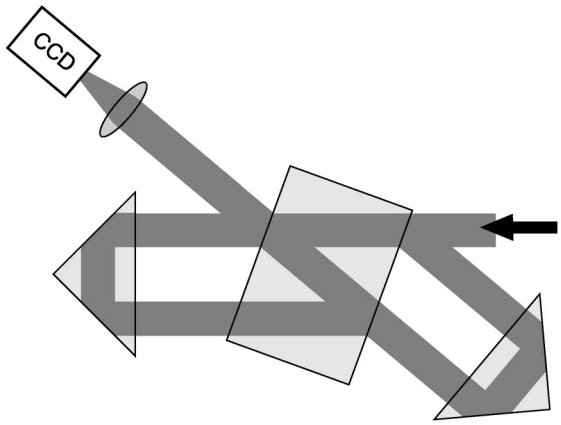

Fig. 8. Optical setup used to measure the relative deflection of two right-angle prisms or corner cubes.

C. Right-Angle Prism and Corner Cube Characterization

We characterized the relative deflection of pairs of right-angle prisms using a scheme similar to the one we used for penta prisms. Because these prisms deflect light back toward the beam splitter, an optical layout analogous with the one we used to measure penta prisms cannot be used—a beam reflected off of one prism would be occluded by the second prism. One approach would be to use a design in which the beams were deflected vertically back to a second beam splitter placed above the first beam splitter. To avoid the complications of multitiered optics, we instead used the layout shown in Fig. 8. In this design a single beam splitter is used to split and recombine the two beams. Unlike the schemes described earlier in this paper, the intensities of the two interfering beams are not precisely balanced in this setup; whereas both paths involve one beam-splitter reflection, the path through the upper prism undergoes two more transmissions through beam-splitter surfaces than the path through the lower prism. Because of the low reflectivity of the uncoated beam splitters, we still achieved nearly 100% fringe contrast. This same setup could also be used to characterize corner cubes.

In addition to the two beams we are interested in, a third beam traveling through the upper prism in the opposite direction can have an effect on the interference pattern. This beam undergoes two additional beam-splitter reflections and is therefore much less intense. When measuring right-angle prisms, the prisms can be tilted vertically to walk this stray beam out of the interference pattern. With the vertical alignment walked off, the distance between the beam splitter and the prisms will have to be adjusted to

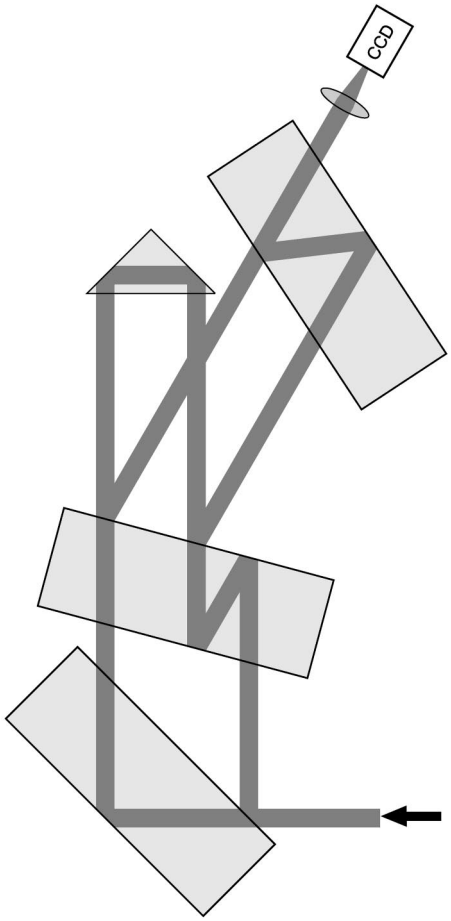

Fig. 9. Optical setup for absolute measurement of right-angle prism and corner cube deflection angles.

achieve good overlap of the interfering beams. As with the penta prism measurements, to measure the difference in the intrinsic deflection angles of two right-angle prisms, we scanned the vertical angle of one of the prisms and then fit the measured relative beam angles to Eq. (10). Using this method we measured the relative deflection angle of pairs of high-quality right-angle prisms. The repeatability of these measurements was similar to what we achieved with our penta prism measurements.

To measure the absolute deflection angle of a single right-angle prism or corner cube we used the scheme illustrated in Fig. 9. Unlike the other schemes presented in this paper, this scheme requires that the beam-splitter angles be chosen carefully. Simpler designs in which one or two beam splitters were used had problems with stray reflections that resulted in interference of more than two paths and unequal intensities of interfering beams. The three-beam-splitter design allows us to control stray reflections but requires a different angle of incidence at each beam splitter. This results in different Fresnel reflection coefficients at each beam splitter. Also, like our scheme for relative measurements of right-angle prisms, in this setup one of the beams undergoes two more transmissions through a beam-splitter surface than the other beam. By carefully choosing the beam-splitter angles, one can make the two pathways overlap and be equal in intensity at the camera. This is easily done with knowledge of the beam-splitter thickness and index of refraction.

We used this method to measure the absolute deflection angles of several high-quality right-angle prisms as well as a low-quality right-angle prism and a high-quality corner cube. The high-quality prisms and the corner cube deflection angles were typically found to deviate from 180 deg by a few microradians. The deflection angle of the inexpensive right-angle prism was found to be much less accurate. Once again we found repeatability at the microradian level.

4. Components Used

For our measurements we used only the prisms under test and parts available in our laboratory. The laser was an inexpensive $\simeq$1 mW helium–neon alignment laser (JDS Uniphase, Model 1507P). Because the prisms and beam splitters did not have reflective coatings, only $\sim$0.01–1% of the laser light reached the camera depending on the type of prisms being measured. Even so we still needed significant attenuation to avoid saturating the camera. The laser had a good spatial mode and a coherence length long enough to produce good interference fringes on the asymmetric Michelson–Morley interferometer mentioned above. A laser with poorer spatial and temporal qualities could also have been used. The required spatial mode can easily be achieved by spatial filtering, especially considering the low power needed. If the two optical paths are made equal within $\sim$1 mm when measuring the prisms, a short-term linewidth of tens of gigahertz would be sufficient to produce high-contrast fringes. Although a short coherence length would not allow collimation to be tested with an asymmetric interferometer, there are many other ways to ensure good collimation.

The camera was a \$156 closed circuit surveillance camera connected to a computer frame grabber card. The low-quality camera resulted in three significant difficulties. First was the camera's nonlinear response. Our camera was not designed for scientific work and its response function was not well calibrated. As a result, in our first measurements the cosine function in Eq. (4) did not oscillate between -1 and 1. We attempted to characterize the camera's response (surveillance cameras usually have a response in which the value of each pixel is proportional to the intensity of light on the pixel raised to some power γ). But we found that, even with a fixed iris setting, at high intensities the signal reported on one pixel depended on the intensity present on other parts of the chip! But for sufficiently low intensities the camera response was fairly linear. So our solution was to reduce light intensities by adding attenuators in front of the camera until the highest value reported at any pixel was 80 counts (out of a maximum of 255 counts for the 8-bit camera).

The other two problems with the camera were related to its low signal-to-noise ratio and to an un-

coated window on the front of the camera. The signal-to-noise ratio problem was overcome by averaging 50 frames to produce each image. This took less than 2 s on our 30 frames/s video camera. The uncoated window affixed to the camera produced low-contrast interference fringes in our data (see Figs. 2 and 3). We were unable to remove this window. But by tilting the camera we were able to make the spatial frequency of these fringes high enough that they did not confuse the fitting routines when fitting the much broader fringes due to the relative angle of the two interfering beams. Note that Eq. (4) was derived under the assumption that the beams strike the camera near to normal incidence. Equation (4) is still approximately correct when we tilt the camera, especially when the camera is tilted around an axis that is nearly perpendicular to the fringes. Tilting our camera, therefore, did not change the way that we analyzed our images, and the residual error due to the camera tilt was negligible.

The lenses and mirrors we used were standard research-quality optics that were already available in the laboratory. Two lenses were used to telescope and collimate the laser beam before entering the interferometer. These had to be of reasonable quality to prevent significant wave-front distortion of the laser. Any distortion due to these lenses is common to both of the interfering beams and should have a reduced effect on the measured fringes. A third lens was used to demagnify the interference pattern to fit onto the camera. This lens simply images the interference pattern. Small wave-front errors at this lens do not have an effect on the measurement, and only its imaging characteristics need to be considered. Like the lenses, the mirrors were employed only before the optical beam was split or after the two paths had been recombined such that wave-front distortions were common to both paths.

After verifying the quality of our parallel-plate beam splitters, these optics were used in the evaluation of the other prisms. Therefore our measurements were limited to the accuracy of the beam splitters. It should be possible to remove this offset by careful characterization of the beam splitters used and by making two sets of measurements with the beam splitters flipped over between them. But given the $\lambda/10$ surface quality of the beam splitters, it is possible that the deflection angles for two different 1 cm sized spots on a beam splitter will differ at the microradian level even if the optic has no overall deflection error. Lowering this systematic error therefore would require either beam splitters with better surface flatness or calibration at the precise locations at which beams enter and leave the beam splitters.

5. Conclusions

We have demonstrated several relatively simple and inexpensive techniques to characterize the deflection angles of parallel-plate beam splitters, penta prisms, right-angle prisms, and corner cubes. We have achieved accuracies at the level of 2 μrad (0.4 arcsec), approaching what is possible in high-end commercial devices. Better results are likely to be possible by calibrating and removing effects due to imperfect beam splitters and by using a higher-quality detector.

We acknowledge the contributions of Rebecca Merrill and Elizabeth Cummings. This research was supported by the Research Corporation and the National Science Foundation.

References

1. J. O. Dickey, P. L. Bender, J. E. Faller, X. X. Newhall, R. L. Ricklefs, J. G. Ries, P. J. Shelus, C. Veillet, A. L. Whipple, J. R. Wiant, J. G. Williams, and C. F. Yoder, "Lunar laser ranging: a continuing legacy of the Apollo program," Science **265,** 482–490 (1994).
2. M. V. Mantravadi, "Newton, Fizeau, and Haidinger interferometers," in *Optical Shop Testing*, 2nd ed., D. Malacara, ed. (Wiley, 1992), pp. 1–50.
3. D. Malacara, "Twyman-Green interferometer," in *Optical Shop Testing*, 2nd ed., D. Malacara, ed. (Wiley, 1992), pp. 51–94.
4. Z. Malacara, "Angle, distance, curvature, and focal length," in *Optical Shop Testing*, 2nd ed., D. Malacara, ed. (Wiley, 1992), pp. 715–742.
5. M. V. Mantravadi, "Lateral shearing interferometers," in *Optical Shop Testing*, 2nd ed., D. Malacara, ed. (Wiley, 1992), pp. 123–172.
6. J. E. Greivenkamp and J. H. Bruning, "Phase shifting interferometers," in *Optical Shop Testing*, 2nd ed., D. Malacara, ed. (Wiley, 1992), pp. 501–598.